JOURNAL OF THERMOPHYSICS AND HEAT TRANSFER
Vol. 10, No. 2, April–June 1996

Thermal Modeling and Analysis of Laser Calorimeters

Z. M. Zhang*
University of Florida, Gainesville, Florida 32611
and
D. J. Livigni,† R. D. Jones,‡ and T. R. Scott§
National Institute of Standards and Technology, Boulder, Colorado 80303

We performed detailed thermal analysis and modeling of the C-series laser calorimeters at the National Institute of Standards and Technology for calibrating laser power or energy meters. A finite element method was employed to simulate the space and time dependence of temperature at the calorimeter receiver. The inequivalence in the temperature response caused by different spatial distributions of the heating power was determined. The inequivalence between electrical power applied to the front and rear portions of the receiver is ≈1.7%, and the inequivalence between the electrical and laser heating is estimated to be <0.05%. The computational results are in good agreement with experiments at the 1% level. The effects of the deposited energy, power duration, and relaxation time on the calibration factor and cooling constant were investigated. This article provides information for future design improvement on the laser calorimeters.

Nomenclature

A = area of the cavity aperture, m^2
A_c = cross-sectional area of the wire, m^2
b = thermopile responsivity, V/K
C = heat capacity, J/K
c = specific heat, J/(kg·K)
E = calibration factor, J/V
F = configuration factor
G = thermal conductance, W/K
h = heat transfer coefficient, W/(m^2·K)
k = thermal conductivity, W/(m·K)
L = length of the wire, m
P = power, W
p = perimeter of the wire, m
S = steady-state responsivity, V/W
T = temperature of the cavity, K
T_a = room temperature, K
T_0 = temperature of the heat sink, K
t = time, s
V = output voltage, V
V_∞ = output voltage at $P = 0$ and $t \to \infty$, V
W = total energy deposited on the calorimeter, J
α = cooling constant, s^{-1}
ε = emissivity
θ = relative temperature ($T - T_0$), K
σ = Stefan–Boltzmann constant, 5.67×10^{-8} W/(m^2·K^4)
τ_w = transmittance of the window

I. Introduction

ELECTRICALLY calibrated calorimeters have been developed during the past 30 years at the National Institute of Standards and Technology as national reference standards for calibrating laser power and energy meters used in industry and research laboratories.[1] These calorimeters operate at or above room temperature and are based on the change of temperature or internal energy of the sensing element by the absorption of optical radiation. As shown in Fig. 1, a laser calorimeter consists of a cavity receiver, a heat sink (whose temperature is maintained constant by a feedback controller), a temperature indicator (such as a series of thermocouples that measure the temperature difference between the receiver and the heat sink using the thermoelectric effect), and an electrical heater that is attached to the receiver to calibrate the response of the thermal sensors. The C-series calorimeters were designed for continuous-wave (CW) laser power and energy measurements in the wavelength range from 0.4 to 2 μm using a fused-silica window.[2,3] The dynamic range is from 0.3 mW to 1 W in power and 0.1 to 30 J in energy. The systematic error is less than 0.5%, and the standard deviation of an electrical calibration is approximately 0.2% over the whole power range.

In recent years, cryogenic radiometers have been developed for measuring laser power and optical radiation with an uncertainty of 0.02%.[4,5] A radiometer uses steady-state response, whereas a calorimeter uses transient response for determination of the deposited heating power or energy. The main advantages of operating at cryogenic temperatures are the reduction of specific heat (which improves the time response), and the increase of thermal diffusivity (which improves the temperature uniformity), by several orders of magnitude from

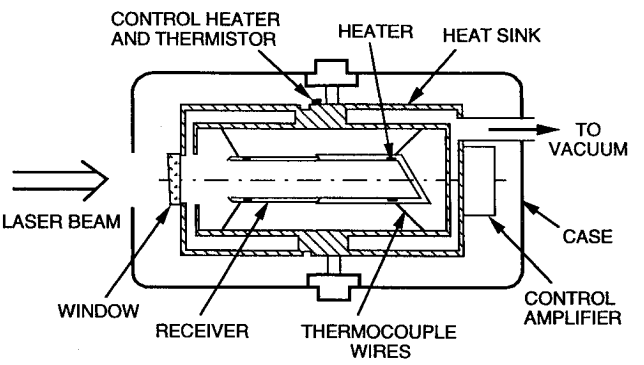

Fig. 1 Cross-sectional schematic of the C-series calorimeters.

Received June 29, 1995; presented as Paper 95-3520 at the 1995 National Heat Transfer Conference, Portland, OR, Aug. 5–9, 1995; revision received Nov. 9, 1995; accepted for publication Nov. 9, 1995.

*Assistant Professor, Department of Mechanical Engineering.
†Electronic Engineer, Sources and Detectors Group of the Optoelectronics Division.
‡Chemist, Sources and Detectors Group of the Optoelectronics Division.
§Supervisory Physicist, Sources and Detectors Group of the Optoelectronics Division.

room temperature to liquid helium temperature for certain materials, such as Cu and Ag. Currently available cryogenic radiometers, however, can measure powers only at or below 1 mW with 0.02% uncertainty.

There is an increasing demand for high-accuracy laser power and energy measurements at power levels greater than 1 mW (see Ref. 5 and papers in the same issue). Therefore, it is necessary to quantitatively assess the existing room-temperature calorimeters. A thorough investigation of the heat-transfer mechanisms in the calorimeters is essential. Theoretical analyses of isoperibol (meaning constant-temperature surroundings) calorimetry were carried out by West and Churney[6] and Johnson.[7] However, neither of these studies was able to model the spatial distribution of temperature because of the complexity of the geometric structure. Mahan et al.[8] used a finite element method (FEM) to study the thermal behavior of infrared (IR) radiometers. Zhang et al.[9] employed an FEM to model the steady-state temperature distribution and the time response of two cryogenic radiometers. These studies lead to several important suggestions on future design changes that would improve the accuracy, sensitivity, and time response of absolute radiometers. Hence, finite element analysis is a useful tool for modeling complicated geometry, and numerical modeling is important to the understanding of the heat transfer mechanisms. In the present work, we apply an FEM to study the steady-state and transient responses of one of the C-series calorimeters, designated as C4-1. The numerical simulations are compared with experiments at different conditions.

II. Analysis

A. Theory of Ideal Calorimetry

An ideal calorimeter would have a uniform cavity temperature as illustrated in Fig. 2, where $T(t)$ is the temperature of the cavity. The cavity exchanges energy with a heat sink, which is maintained at T_0, through G_a. The cavity can also interact with, for example, the window at temperature T_w (which depends on room temperature), through G_b. Although actual calorimeters vary substantially from this simplified model, it is useful to discuss calorimetric theory starting with this model. In a steady state ($t \to \infty$) with zero input power, the temperature of the cavity is

$$T(t \to \infty) = T_\infty = (G_a T_0 + G_b T_w)/G \tag{1}$$

where $G = G_a + G_b$. Since the thermopile output depends on the temperature difference between the cavity and the heat sink, it is convenient to define a new temperature parameter:

$$\theta = T - T_0 \tag{2}$$

Equation (1) can then be written as

$$\theta_\infty = \theta_w G_b/G \tag{3}$$

If the thermopile's responsivity is b, then the output voltage for zero input power is

$$V_\infty = b\theta_\infty \tag{4}$$

which is called the baseline. The baseline is an important parameter for the data reduction, and its stability is crucial for measurement and calibration, especially at low input powers.

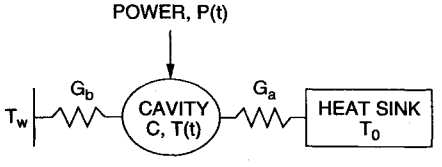

Fig. 2 Model of an ideal calorimeter.

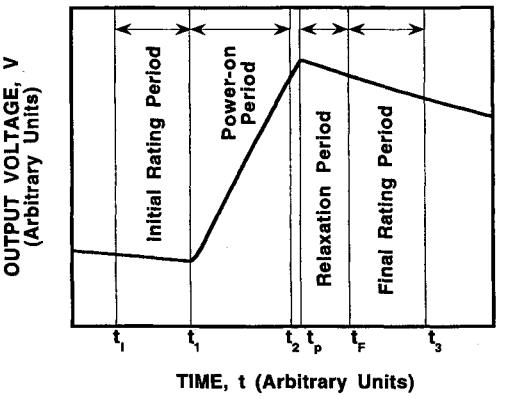

Fig. 3 Illustration of the history of the thermopile output.

The steady-state thermopile output for a constant input power P is

$$V - V_\infty = SP \tag{5}$$

where S is given by

$$S = b/G \tag{6}$$

In many systems, a long time is needed to achieve a steady state because of the massive cavity required to obtain an absorptivity approaching unity. In the actual measurement, the thermopile output is recorded over a period of time. The history of the thermopile output voltage is illustrated in Fig. 3,[2,3,6,7] where t_i is the time at the beginning of the initial rating period (the rating period will be explained later), t_1 is the time when the power is turned on (either electrical current is supplied to the heating element or the shutter is open for the laser beam to enter the cavity), t_2 is the time when the power is turned off, t_p is the time when the thermopile output reaches its peak value, t_F is the time at the beginning of the final rating period, and t_3 is the time at the end of the final rating period. The time between t_p and t_F is called the relaxation period. In the simple model given in Fig. 2, $t_p = t_2$. In actual systems, such as that shown in Fig. 1, there is a delay between t_p and t_2. The total energy that is applied to the cavity during the power-on period is determined by the change in the internal energy plus the energy transferred from the cavity to the heat sink, i.e.,

$$W = \frac{1}{b} C(V_F - V_I) + \frac{1}{b} G \int_{t_I}^{t_F} (V - V_\infty)\, dt \tag{7}$$

where the temperature difference is written in terms of the measurable quantity, the voltage output from the thermopile. The cooling constant α is defined as the reciprocal of the $1/e$ time constant, $\alpha = G/C$. Equation (7) can be rewritten as

$$W = E\left[(V_F - V_I) + \alpha \int_{t_I}^{t_F} (V - V_\infty)\, dt\right] \tag{8}$$

where E ($=C/b$) is called the calibration factor since it is determined by electrical calibration, and the quantity in the brackets is called the corrected (temperature) rise. This is the working equation for isoperibol calorimetry.[6,10]

An important concept in isoperibol calorimetry is the rating period. For the model in Fig. 2, if the cavity is first raised to a temperature higher than that of the heat sink, the cooling equation is

$$\frac{d\theta}{dt} = -\alpha(\theta - \theta_\infty) \tag{9}$$

When the temperature of the cavity is not uniform, and the temperature variation of the cavity is much less than the temperature difference between the cavity and the heat sink, Eq. (9) is a good approximation for the observed temperature (the average temperature at which the measurement is taken) after a certain time. A rigorous derivation was given by West and Churney.[6] By definition, a rating period is a period when Eq. (9) holds for every point on the cavity. The time needed for a calorimeter to reach a rating period is greater than all of the relaxation times, except for the relaxation time approximately equal to C/G. The initial and final rating periods for a typical measurement are shown in Fig. 3. Two criteria must be met before Eqs. (8) and (9) can be applied: first, the thermal coupling between different parts of the cavity must be much stronger than that between the cavity and the heat sink; second, G, C, and b must not be strong functions of temperature. Since at cryogenic temperatures the thermophysical properties of materials depend strongly on temperature, it is not possible to build a cryogenic calorimeter based on the same techniques.

The initial and final rating periods are used to determine the cooling constant and the baseline, as described by West.[10] Then the corrected rise is evaluated. The calibration factor is determined with electrical heating when the energy deposited on the heater is measured precisely. This calibration factor is used to determine the laser energy.

Johnson[7] investigated the temperature (output voltage) history of C-series calorimeters and compared the one-time-constant model (in which the output is an exponential function of time) to a two-time-constant model (in which the output is the sum of two exponential functions of time with different time constants). The two-time-constant model showed some advantages over the one-time-constant model at the beginning of the power-on period and the relaxation period. The results in the rating period obtained from the two models, however, are essentially the same since the term with a short time constant becomes negligibly small after the relaxation period.

B. Configuration of the C4-1 Calorimeter

The receiver, shown in Fig. 1, consists of two thin walls jointed in the middle. The walls are made of electroformed Ag with a total thickness of approximately 120 μm. The length of the cavity is $\approx$8.5 cm and the diameter of the inner cylinder is $\approx$2 cm. The mass of the two cylindrical walls is 16.24 g. The mass of the joint between the inner and outer walls is $\approx$1.59 g. The three surfaces of the two walls are coated with Au, whereas the inner surface is coated with a black paint. The thickness of the Au coating is of the order of 100 nm and its mass is negligible. The total mass of the black paint is between 0.2–0.4 g (about 25 μm thick). The heaters are made of Cu–Mn–Ni alloy wires (1 m long and 75 μm in diameter). The mass of the heater wires is <10 μg, much less than the mass of the cavity. The electrical leads of the heaters are made of Cu and specially arranged to reduce inequivalence, as described in Ref. 3. The mass of solder and epoxy is estimated to be about 0.2 g. The heat-sink temperature is feedback controlled to near 35°C with a rms fluctuation of 1 mK.

The thermopile is made of 16 pairs of type-E thermocouples, whose positive thermoelement is made of a Ni–Cr alloy and negative thermoelement is made of a Cu–Ni alloy.[11,12] The thermophysical properties of the materials used in the calorimeter that are important for the analysis are listed in Tables 1 and 2.[13–17] The sensitivity is $\approx$62 μV/K for each junction at temperatures from 35 to 40°C.[12] Hence, the thermopile sensitivity is $b \approx 0.992$ mV/K. The responsivity of the thermocouple changes approximately 0.4% for temperatures from 35 to 40°C. The tenth-order polynomial recommended in Ref. 12 was used to compute the voltage response to a temperature difference in the numerical model. The thermocouples were attached to the receiver using epoxy. In addition, a 50-μm-thick mica layer was used as an electrical insulator between the thermocouple junctions and the wall. The thermal conductivity of mica is $\approx$0.005 W/(cm·K).[18] The thermal resistance of the thermocouple leads is of the order of 10^5 W/K, whereas thermal resistance of a mica layer with 5 × 5 mm^2 area is only 4 W/K. Therefore, the temperature drop because of the mica layer is negligibly small.

Table 1 Density, thermal conductivity, and specific heat

Material	ρ, g/cm^3	k, W/(cm·K)	c, J/(g·K)
Ag	10.5	4.27	0.236
Cu	8.96	4.00	0.385
Cu–Ni alloy	8.9	0.23	0.38
Ni–Cr alloy	8.6	0.19	0.43

Table 2 Emissivity

Material	Total hemispherical ε
Au coating	0.02
Varnish	0.80
Epoxy	0.73
Black paint	0.93
Fused silica	0.75

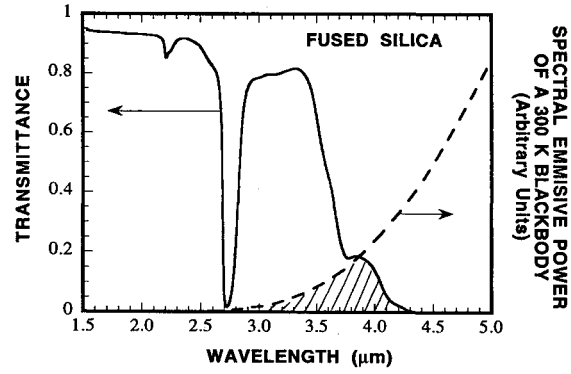

Fig. 4 Spectral transmittance of the window.

The heat capacity calculated from 17.8 g of Ag is 4.2 J/K, resulting in a calibration factor $E = C/b = 4.24$ J/mV. This falls within the range determined experimentally for three C-series calorimeters. In the thermal modeling, the peripheral materials are neglected since the uncertainty in the estimated mass of the Ag is greater than the total mass of the other materials. The experimentally determined cooling constant is $\alpha \approx 1.23$ ks^{-1}, indicating that the total thermal conductance between the cavity and the heat sink is $G \approx 5.2$ mW/K.

C. Window Transmittance

We have examined the transmittance of the window to understand how room temperature affects the cavity temperature. The window was made of 6-mm-thick fused silica. A Fourier-transform infrared spectrometer was used to measure the transmittance of the window for wavelengths from 1.6 to 25 μm. The transmittance below 5 μm is shown in Fig. 4. The transmittance from 5 to 25 μm is essentially 0. Our measurement is consistent with the existing data for fused silica.[15] The transmittance of an 8 mm thickness of fused silica is nearly 0 at wavelengths from 5 to 100 μm, and less than 5% at wavelengths from 100 to 200 μm.[15] From Planck's blackbody distribution function, the fraction of the radiated power from a 300-K blackbody is less than 0.5% for wavelengths longer than 100 μm and less than 0.1% for wavelengths longer than 200 μm.[19] Therefore, the total transmittance at wavelengths longer than 5 μm is less than 0.1%. The fraction of radiated power at wavelengths shorter than 5 μm is only 1%. The total transmittance at wavelengths shorter than 5 μm can be obtained by integrating the products of Planck's distribution

function, divided by σT^4, and the spectral transmittance (as indicated by the shaded area in Fig. 4), where σ is the Stefan–Boltzmann constant. This yields a transmittance of $\approx$0.1%. Therefore, the total transmittance of the window is $\tau_w < 0.2\%$. The configuration factor of the aperture of the cavity to the window is calculated to be $F \approx 0.086$.[19] Hence, the net power transmitted through the window in the absence of any optical source is $\tau_w\sigma AF(T^4 - T_a^4)$, < 4 μW. This power can only change the cavity temperature by less than 1 mK, which is insignificant and varies little with changes of room temperature. Therefore, in the numerical model, the window can be treated as totally opaque to ambient radiation. Furthermore, the change of cavity temperature because of the room-temperature variation is not caused by radiation transmitted through the window, but by a change of the window temperature.

The transmittance of the window at the laser wavelength must be accurately determined. A method for accurate determination of the transmittance was discussed in Ref. 2 with a reported uncertainty of 0.12%.

D. Heat Flow Paths

The cavity exchanges heat with the heat sink or the window through conduction and radiation. The high vacuum ($<10^{-4}$ Pa) inside the calorimeter virtually eliminates convective heat transfer. For cryogenic radiometers, the radiative heat transfer from the receiver to the heat sink is negligibly small compared to the conductive heat transfer.[9] For room-temperature calorimeters, however, the heat transfer from the receiver to the heat sink is mainly by radiation. The purpose of the analysis in this section is to understand the heat transfer mechanisms, which will facilitate the development of the numerical model. The estimated thermal conductances associated with the different mechanisms are used to check the numerical modeling.

Radiation between the cavity and the window determines the baseline. The window temperature is different from the heat-sink temperature because of the heat exchange with the room. The thermal conductance between the aperture of the cavity and the window can be estimated by $4\varepsilon_w AF\sigma T_0^3 \approx 0.12$ mW/K, where $\varepsilon_w \approx 0.75$ is the total hemispherical emissivity of the window, assuming that the emissivity of the cavity is 1 and that the temperatures of the cavity and the window are close to that of the heat sink.

The thermal conductance (by radiative transfer) between the aperture of the receiver and the heat sink is estimated by $4A(1 - F)\sigma T_0^3 \approx 1.75$ mW/K, assuming that the emissivity of the cavity is 1.

The emissivity of Au is taken to be 0.02[16,17] to estimate the radiation from the outside surface of the cavity to the heat sink. The total area of the outside surface is approximately 60 cm^2, yielding a thermal conductance of $\approx$0.8 mW/K.

Epoxy was used to attach the thermocouple junctions to the receiver. There are eight epoxy pats, and each has an area of $\approx$0.33 cm^2. The emissivity of the epoxy is taken to be 0.73.[16] The thermal conductance between the epoxy pats and the heat sink is $\approx$1.28 mW/K. Hence, radiation heat transfer through the epoxy pats accounts for approximately one-quarter of the total heat transfer from the receiver to the heat sink, which was not realized by earlier investigators.

Thermal conduction through the wires is insignificant compared to radiation. This is because of the lower thermal conductivity of the thermocouple wires and the long Cu leads of the heaters. The diameter of all the wires is $\approx$127 μm. The thermocouple wires are $\approx$2.5 cm long and the Cu leads are arranged in a Y shape with $\approx$4-cm-long branches. There is a varnish insulation layer around the wires. Although the thermal conductivity of the varnish is much lower than that of the metallic wires, it has a large emissivity and the radiation from the wire may enhance the heat transfer by the wires, especially for the alloy thermocouple wires that have a low thermal conductivity. This effect is estimated by[20]

$$\frac{d^2T_l}{dx^2} - \frac{hp}{kA_c}(T_l - T_0) = 0 \qquad (10)$$

where $h = \varepsilon_l\sigma(T_l + T_0)(T_l^2 + T_0^2)$ is the radiative heat transfer coefficient, T_l is the temperature of the wire, and x is the coordinate along the wire. Equation (10) assumes that the radiation exchange between the wire and the cavity is much less than that between the wire and the heat sink, because both the surface area and the emissivity of the cavity are much less than those of the heat sink. The effective thermal conductance is the effective heat-flow rate at the cavity divided by the temperature difference between the cavity and the heat sink. If the end temperature at the heat sink is fixed, that is, $T_l(x = L) = T_0$, then the effective thermal conductance is[20]

$$G_{\text{eff}} = (kA_c/L)[\sqrt{(hpL^2/kA_c)}/\tanh\sqrt{(hpL^2/kA_c)}] \qquad (11)$$

The value in the brackets of Eq. (11) is $\approx$2.4 for the Cu–Ni wires and $\approx$2.9 for the Ni–Cr wires, indicating that radiation has a significant effect on the heat transfer via the wires. For the Cu leads, the effect of radiation is negligibly small. A more rigorous solution can be found in the work of Cheng et al.[21] An effective thermal conductivity is used in the numerical modeling, which is equal to $G_{\text{eff}}L/A_c$. The estimated thermal conductances of the Cu–Ni wires, Ni–Cr wires, and Cu leads at $T_l \approx T_0 = 35$°C are approximately 0.42, 0.41, and 0.35 mW/K, respectively. The estimated total thermal conductance between the receiver and the heat sink is $\approx$5.13 mW/K.

III. Numerical Modeling

A commercial finite element software was employed to model the heat transfer in the calorimeter, based on the analysis discussed in the previous section. A three-dimensional model was used to model the radiation since the bottoms of the cylindrical walls are inclined. The finite element model is shown in Fig. 5. The cylindrical walls are modeled with shell elements, the thermocouple wires and Cu leads are modeled with line elements, and the joint between the inner layer and outer layer of the cavity is modeled with solid elements, all of which are three dimensional. The heater leads are bent arbitrarily to give the right length. The cylindrical wall is circularly divided into 16 parts, and the element length along the cavity is less than or equal to 5 mm.

The window and heat sink are assumed to be at constant temperatures. An important part of the model is the radiative heat transfer between the cavity and the heat sink: The configuration factors between the elements in an enclosure are stored in a radiation matrix for calculation of the radiative heat transfer between the inner cavity and the window or the heat sink. To have a closed model (an enclosure), an artificial cylindrical shell with an emissivity equal to 1 is located between the window and the cavity. The emissivity of the black paint is approximately 0.93, while its absorptance to radiation at wavelength from 0.3 to 2 μm is between 0.96–0.98 (Refs. 16 and 22). The radiation between the epoxy pats and the heat sink is modeled using radiation links, which are two node elements for modeling radiation between two points. The radiation flux between the Au-coated outside surface and the heat sink is simplified by $4\sigma[(T + T_0)/2]^3(T - T_0)$. This allows us to use convective boundary conditions to model the radiative heat transfer. The error in the total heat flux calculation caused

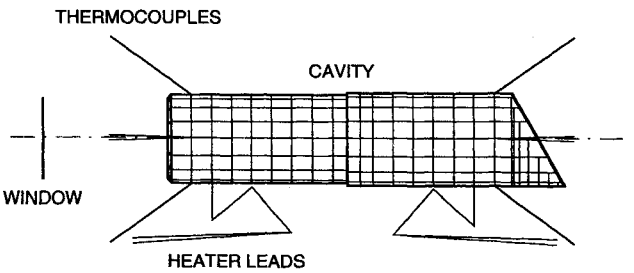

Fig. 5 Numerical model.

by this approximation is less than 0.005% for $|T - T_0| \leq 10$ K. There are 1316 elements and 8018 nodes in the model. Because of the large memory used by the radiation matrix, we were not able to refine the mesh further with the available computer resources. The computation was run on a workstation with a speed of 125-million floating-point operation per second. The steady-state solution requires three iterations to converge to less than 10 μK between succeeding iterations and takes about 1 min of CPU time. In the transient modeling, the effect of time step size on the results was investigated. A time step of 0.8 s was chosen because the difference between a 1.6-s time step and a 0.8-s time step is less than 0.1%. A fixed time step was used, except for those immediately following the power-on and power-off time, where a time step of 1 ms was used. Each step takes 3–4-s CPU time. The Crank–Nicolson scheme was used to integrate the governing equation with respect to time, and the Newton–Raphson iteration was used to solve the nonlinear equations.[23]

A. Steady-State Results

As shown in Fig. 6, the baseline depends on room temperature. A linear fit to the experimental data showed that the sensitivity of baseline to room temperature T_a is $dV_\infty/dT_a \approx 5$ μV/K, and $V_\infty = -77$ μV at $T_a = 21$°C. The negative baseline implies that the receiver's temperature is less than that of the heat sink. There is large scatter in the data: the deviation from the fitted line can be as large as 4 μV. Since the heat-sink temperature is controlled and the window is opaque, room temperature can affect the cavity temperature only through a change in the window temperature. The window exchanges heat with the room via convection and radiation, while it exchanges heat with the heat sink and cavity via conduction and radiation. The scatter may be caused by different convection conditions in the room and by different wall temperatures of the room. A baseline change of 4 μV corresponds to ≈4 mK change of the cavity temperature ($b \approx 0.992$ mV/K). We have computed the baseline as a function of the window temperature. The baseline was calculated from the average temperature of the eight nodes outside the cavity where the thermocouple hot junctions are located. For a heat-sink temperature T_0 of 35°C, a baseline V_∞ of -77 μV corresponds to a window temperature T_w of 31.5°C, indicating that the window temperature is closer to the heat-sink temperature than to room temperature. This implies that the conduction between the window and the heat sink is greater than the convection between the window and the room. Based on the previous analysis, it is suggested that the stability of room temperature should be improved and radiation baffles may be installed between the calorimeter and the walls.

The steady-state responsivity is computed for both the front heater and rear heater. Figure 7 compares the calculated and measured steady-state responsivities. The experiment takes 8000 s, about 10 times the time constant, to achieve 99.995% of the steady-state value. The calculated responsivity agrees with that obtained from the experiments within 1%. This agreement is satisfactory considering the uncertainty in the thermophysical properties and the geometry. The responsivity decreases with increasing power because of the strong nonlinearity of radiative heat transfer. From $P = 1$ to 50 mW, the responsivity decreases by ≈2.5%. Because of the opening of the receiver, the radiative thermal coupling between its front portion and the heat sink is stronger than that between its rear portion and the heat sink. Hence, the responsivity is smaller with the front heater. The inequivalence between the front heater and the rear heater is ≈1.6% from experiments and ≈1.8% from calculations. This agreement is satisfactory. There is a large uncertainty in the experiment when $P \approx 3.5$ mW. This could be caused by a change in the window temperature as a result of the room-temperature variation. If room temperature changes 1 K, the baseline will change by 5 μV, resulting in an error of 0.7% in the measured steady-state responsivity

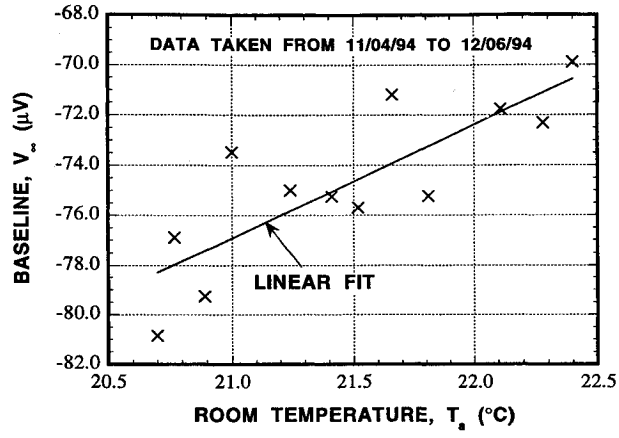

Fig. 6 Correlation between the baseline and the room temperature.

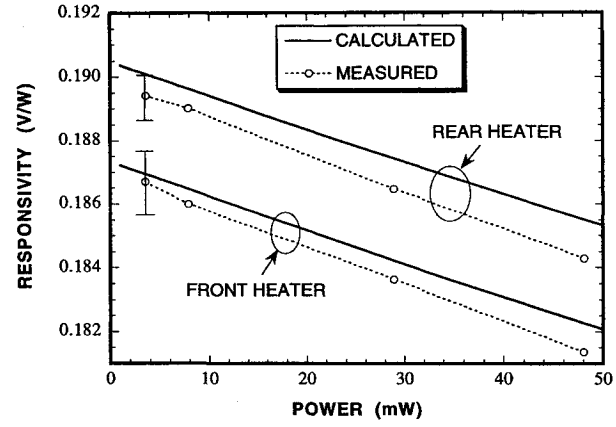

Fig. 7 Steady-state responsivity for both the front and rear heaters. The error bars indicate the standard deviation for three runs with a 3.5-mW power. The standard deviation for powers greater than 7.9 mW is less than 0.1%.

for $P \approx 3.5$ mW. Even though the air temperature is the same, different convection conditions and wall temperatures may cause a baseline variation of several microvolts. Hence, it is important to control the laboratory environment, in particular for low-power measurements ($P < 5$ mW). One of the advantages of the calorimetric technique is that the total measurement time is less than the thermal time constant since it uses the transient data to determine the total energy. The baseline variation should be less significant in the transient measurements.

The laser power is presumably not strong enough to cause a phase transition in any material. To determine the inequivalence between the laser heating and the electrical heating, the distribution of laser power must be known. The absorptance of the black paint is greater than 0.96 (Ref. 22). We have estimated the inequivalence by numerically testing two extreme cases. In one case, all of the power was deposited to the central area (<5 mm in diameter) of the ellipsoid at the bottom of the cavity. The results agree with that of the rear heater within 0.01% for $P = 5$ mW. In the other case, 96% of the power was deposited to the bottom of the cavity and 4% of the power was deposited to the front heater location. This yields an upper bound of the inequivalence of 0.05% between laser heating and electrical heating using the rear heater. The loss from the aperture of the cavity was determined from experiments of West and Schmidt[22] to be 0.016 ± 0.026%.

B. Transient Results

The temperature histories are shown in Fig. 8 for different power-on times with the rear heater. The temperature near the

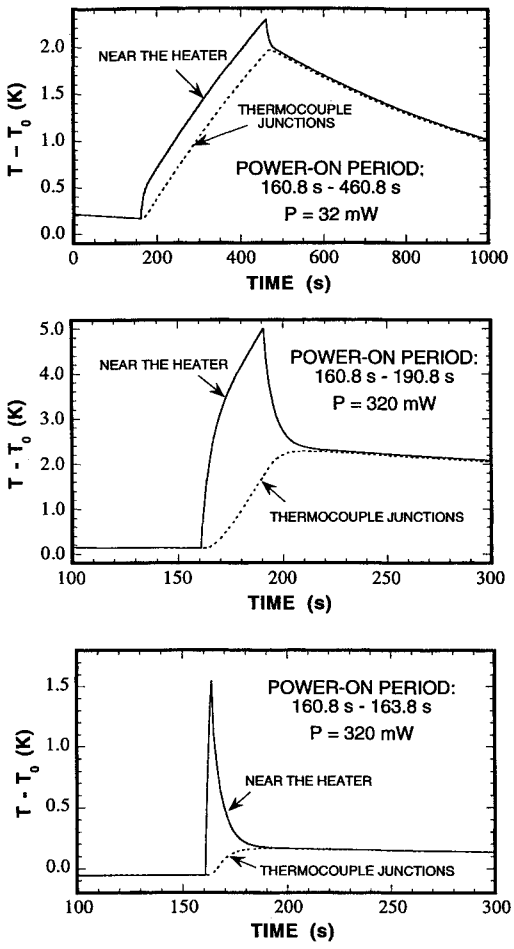

Fig. 8 Predicted temperature rise and fall curves at T_0 = 35°C and T_w = 31.5°C, where the solid curves are for the node near the heater and the dotted curves are the average temperature of the eight nodes of the thermopile hot junctions.

heater increases as the power is turned on and reaches its maximum as the power is turned off. The average temperature of the eight nodes that represent thermocouple junctions on the outside wall of the cavity is also shown. It increases slowly and continues to increase for a short time after the power is turned off (the time lag is $t_p - t_2$, see Fig. 3). The temperatures fall into the same curvature in a short time after the power is turned off. When all of the temperatures on the calorimeter exponentially decay with the same cooling constant, the calorimeter is in a rating period. The modeling results can help determine the relaxation time and the rightness of the rating-period approximation for a particular calorimeter. The time lag $t_p - t_2$ does not depend on the power, but rather, depends on the power duration $t_2 - t_1$. The shorter the power duration, the longer the time lag.

The temperature difference between the cavity and the heat sink was correlated to the voltage output using a tenth-order polynomial.[12] The time-dependent voltage was used in the computer program, developed for processing experimental results, to yield the calibration factor and the cooling constant. The basic principles of the program are described in Ref. 10. The initial and final rating periods are used to calculate the cooling constant and baseline. The corrected rise, the value in the bracket of Eq. (8), is then evaluated. The calibration factor is the ratio of the deposited energy to the corrected rise. The cooling constant and calibration factor for various conditions are shown in Fig. 9 for both experiments and modeling results.

The cooling constant obtained from the modeling is ≈1% less than that obtained from experiments. The steady-state modeling (Fig. 7) shows that the calculated thermal conductance is ≈0.5% lower than the experimental value. Therefore, the estimated heat capacity in the modeling should be ≈0.5% greater than the actual value. The cooling constant is almost the same for both front heater and rear heater. The cooling constant α may be obtained for different nodes by modeling the thermopile junctions at different locations; α depends little on the location (<0.03%), while the calibration factor E strongly depends on the location (up to 7%). This suggests that the cooling constant is an intrinsic parameter of the calorimeter.

The cooling constant increases with the deposited energy because of an increase of G with temperature. For the same energy, α is insensitive to the power-on time. The dependence of α on temperature suggests that the cooling curve is not a simple exponential function. The use of an exponential function causes an error in the baseline. For example, the baseline obtained from the rating periods is ≈ −73 μV for 32-mW power and 300-s duration. This is 2 μV higher than that determined from the steady-state modeling (≈ −75 μV), implying an offset of 0.16% in the corrected rise. The error in the determination of the laser energy should be less than 0.16% since the offset appears in both the calibration and measurements. The error increases as the energy increases.

The E obtained from the modeling is ≈1.5% greater than that from experiments, as seen in Fig. 9b. The trends, however, agree well between the modeling and experiments. Because of the temperature gradient in the calorimeter, E depends not only on the heat capacity, but also on the thermal conductance and cooling constant. The E for the front and the rear heaters differs by 1.7%, which is consistent with the steady-state results. The greater the cooling constant, the greater the corrected rise and the lower the calibration factor. With increasing energy E decreases and α increases. There is little dependence on the power duration by E. The maximum difference in E is <0.03% for power duration from 300 s down to 3 s. This suggests that the calorimeter is immune to power fluctuations and can be used to measure the total energy, even when the laser power is not stabilized.

A relaxation time (see Fig. 3) of 48 s was used in the previous calculation, since it yields a minimum calibration factor

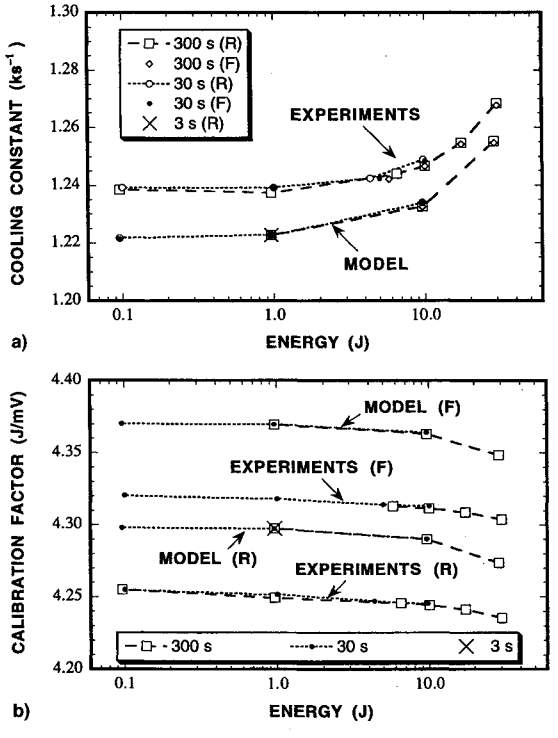

Fig. 9 Comparisons between experiments and theory (where F refers to the front heater and R refers to the rear heater): a) cooling constant and b) calibration factor.

for a power duration of 300 s. The effect of relaxation time on the cooling constant and the calibration factor was investigated by using relaxation times of 20, 48, 80, and 120 s. The change in α is <0.1% and the change in E is <0.01% in all cases. Hence, a relaxation time of 48 s is appropriate for practical applications.

IV. Conclusions and Recommendations

Both steady-state and transient temperature distributions have been modeled using a finite element technique. The results agree with experiments at the 1% level.

Changes in room temperature affect the baseline through a change of the window temperature. The dependence of the baseline on the window temperature has been predicted. Better control of room temperature is required to reduce the baseline variation.

The inequivalence between the front heater and rear heater has been modeled and is consistent with experimental results. The inequivalence between the front heater and rear heater is ≈1.7% in both the steady-state responsivity and the calibration factor. The inequivalence between the laser and the rear heater is estimated to be less than 0.05% (not including the uncertainty in the transmittance of the window).

Radiation accounts for ≈3/4 of the heat transfer between the calorimeter cavity and the heat sink. The thermal conductance and cooling constant depend on temperature. Although the rating-period theory is a good approximation, the cooling curve is not a simple exponential function of time because the cooling constant depends on temperature. This can cause an error in the corrected rise of 0.16% for an energy of 10 J. A more complicated calibration and data processing algorithm would be needed to compensate for the cooling constant variation. The calibration factor depends not only on the heat capacity, but also on the energy and where the energy is deposited. Both the cooling constant and the calibration factor depend little on the power duration, indicating that calorimeters are immune to power fluctuations.

Acknowledgments

The authors thank Hai Tang of the National Institute of Standards and Technology and Abed Khaskra of Mallett Technology, Inc., for their technical support in the use of the software.

References

[1]Scott, T. R., "NBS Laser Power and Energy Measurements," *Laser Beam Radiometry*, edited by A. A. Sanders, *Proceedings of the Society of Photo-Optical Instrumentation Engineers*, Vol. 888, 1988, pp. 48–54.

[2]West, E. D., Case, W. E., Rasmussen, A. L., and Schmidt, L. B., "A Reference Calorimeter for Laser Energy Measurements," *Journal of Research of the National Bureau of Standards*, Vol. 76A, No. 1, 1972, pp. 13–25.

[3]West, E. D., and Case, W. E., "Current Status of NBS Low-Power Laser Energy Measurement," *IEEE Transactions on Instrumentation and Measurement*, Vol. 23, No. 4, 1974, pp. 422–425.

[4]Foukal, P. V., Hoyt, C., Kochling, H., and Miller, P., "Cryogenic Absolute Radiometers as Laboratory Irradiance Standards, Remote Sensing Detectors, and Pyroheliometers," *Applied Optics*, Vol. 29, No. 7, 1990, pp. 988–993.

[5]Houston, J. M., Cromer, C. L., Hardis, J. E., and Larason, T. C., "Comparison of the NIST High Accuracy Cryogenic Radiometer and the NIST Scale of Detector Spectral Response," *Metrologia*, Vol. 30, No. 4, 1993, pp. 285–290.

[6]West, E. D., and Churney, K. L., "Theory of Isoperibol Calorimetry for Laser Power and Energy Measurements," *Journal of Applied Physics*, Vol. 41, No. 6, 1970, pp. 2705–2712.

[7]Johnson, E. G., Jr., "Evaluating the Inequivalence and a Computational Simplification for the NBS Laser Energy Standards," *Applied Optics*, Vol. 16, No. 8, 1977, pp. 2315–2321.

[8]Mahan, J. R., Kowsary, F., Tira, N., and Gardiner, B. D., "Transient Conduction-Radiation Analysis of an Absolute Active Cavity Radiometer Using Finite Elements," *International Symposium on Thermal Problems in Space-Based Systems*, edited by F. Dobran and M. Imber, American Society of Mechanical Engineers, HTD-Vol. 83, New York, pp. 39–47.

[9]Zhang, Z. M., Datla, R. U., Lorentz, S. R., and Tang, H. C., "Thermal Modeling of Absolute Cryogenic Radiometers," *Journal of Heat Transfer*, Vol. 116, No. 4, 1994, pp. 993–998.

[10]West, E. D., *Data Analysis for Isoperibol Laser Calorimetry*, NBS TN 396, U.S. Government Printing Office, Washington, DC, 1971.

[11]*Manual on the Use of Thermocouples in Temperature Measurement*, 4th ed., American Society for Testing and Materials, Philadelphia, PA, 1993, Chap. 3.

[12]Burns, G. W., Scroger, M. G., Strouse, G. F., Croarkin, M. C., and Guthrie, W. F., *Temperature-Electromotive Force Reference Function and Tables for the Letter-Designated Thermocouple Types Based on the ITS-90*, National Inst. of Standards and Technology Monograph 175, U.S. Government Printing Office, Washington, DC, 1993, pp. 101–105.

[13]Touloukian, Y. S., Powell, R. W., Ho, C. Y., and Klemens, P. G., "Thermal Conductivity: Metallic Solids," *Thermophysical Properties of Matter*, Vol. 1, IFI/Plenum, New York, 1970, pp. 68–81 for Cu, pp. 340–348 for Ag, pp. 561–567 for Cu–Ni alloys, and pp. 697–699 for Ni–Cr alloys.

[14]Touloukian, Y. S., and Buyce, E. H., "Specific Heat: Metallic Solids," *Thermophysical Properties of Matter*, Vol. 4, IFI/Plenum, New York, 1970, pp. 208–212 for Ag, pp. 51–61 for Cu, pp. 392–397 for Ni–Cr alloys, and pp. 398–402 for Cu–Ni alloys.

[15]Touloukian, Y. S., and DeWitt, D. P., "Thermal Radiative Properties: Nonmetallic Solids," *Thermophysical Properties of Matter*, Vol. 8, IFI/Plenum, New York, 1972, pp. 403–426.

[16]Touloukian, Y. S., DeWitt, D. P., and Hernicz, R. S., "Thermal Radiative Properties: Coatings," *Thermophysical Properties of Matter*, Vol. 9, IFI/Plenum, New York, 1972, pp. 651–654 for Au, pp. 532–540 for the black paint, and p. 1120 for epoxy.

[17]Weast, R. C., and Astle, M. J. (eds.), *CRC Handbook of Chemistry and Physics*, 60th ed., CRC Press, Boca Raton, FL, 1980, p. E-393.

[18]Touloukian, Y. S., Powell, R. W., Ho, C. Y., and Klemens, P. G., "Thermal Conductivity: Nonmetallic Solids," *Thermophysical Properties of Matter*, Vol. 2, IFI/Plenum, New York, 1970, pp. 823–825.

[19]Siegel, R., and Howell, J. R., *Thermal Radiation Heat Transfer*, 3rd ed., Hemisphere, Washington, DC, 1992, Chaps. 2 and 6.

[20]Incropera, F. P., and DeWitt, D. P., *Fundamentals of Heat and Mass Transfer*, 2nd ed., Wiley, New York, 1985, Chap. 3.

[21]Cheng, S. X., Ge, X. S., Yao, C. C., Gao, J. W., and Zhang, Y. Z., "Research on the Validity of the Steady-State Calorimeter for Measuring the Total Hemispherical Emissivity of Solids," *Measurement Science and Technology*, Vol. 4, No. 5, 1993, pp. 721–725.

[22]West, E. D., and Schmidt, L. B., "Spectral-Absorptance Measurements for Laser Calorimetry," *Journal of the Optical Society of America*, Vol. 65, No. 5, 1975, pp. 573–578.

[23]Reddy, J. N., *An Introduction to Finite Element Method*, McGraw–Hill, New York, 1984, Chaps. 2–4.